

# Violin modeling

HW 1

Federico Capitani (matr. 286822)

Nicola Antonio Magno (matr. 259037)

Gianluigi Vecchini (matr. 273131)

Michele Zanardi (matr. 280928)

Musical Acoustics



**POLITECNICO**  
MILANO 1863

January 18, 2026

### a. Circular plate eigen-frequencies

We start our study from a simplified model, where the soundboard is a circular flat plate, whose radius is  $a = 13.15$  cm and the thickness  $h = 4$  mm. The plate is made by an isotropic material, with the Young modulus equivalent to that of the Sitka spruce along the longitudinal dimension  $E = 12$  GPa ([1]), the Poisson coefficient  $\nu = 0.32$  and the density  $\rho = 400 \frac{\text{kg}}{\text{m}^3}$ . Considering the free edge boundary condition we calculate the first five eigen frequency using:

$$c_L = \sqrt{\frac{E}{\rho(1-\nu^2)}} = 5781.22 \frac{\text{m}}{\text{s}} \quad f_{20} = 0.2413 \cdot c_L \cdot \frac{h}{a^2} = 322.69 \text{ Hz}$$

$$f_{01} = 1.73 \cdot f_{20} = 558.25 \text{ Hz} \quad f_{30} = 2.328 \cdot f_{20} = 751.22 \text{ Hz}$$

$$f_{11} = 3.91 \cdot f_{20} = 1261.72 \text{ Hz} \quad f_{40} = 4.11 \cdot f_{20} = 1326.25 \text{ Hz}$$

Where  $c_L$  is the velocity of propagation of quasi longitudinal waves in thin plates.

### b. Shell plate eigen-frequencies

We now consider an arched plate. The depth of the spherical cap shell is  $H = 15$  mm. The eigen frequency of the lowest mode of the shell can be predicted using the theoretical equation that relates the lowest frequency of the plate to the one of the shell:

$$\frac{f_{\text{shell}}}{f_{\text{plate}}} = \left[ \frac{1}{1-\nu^2} \left( \frac{\mu}{\mu_0} \right)^4 + \frac{48}{\mu_0^4} \left( \frac{H}{h} \right)^2 \right]^{1/2} = 5.23 \quad \Rightarrow \quad f_{\text{shell}} = 1687.67 \text{ Hz}$$

Where  $\mu \approx 3$  rad for free edges shells in which  $H$  is comparable to  $h$  and  $\mu_0 = k \cdot a$  can be found using the dispersive equation for bending waves  $\mu_0 = \sqrt{\frac{\sqrt{12}\omega}{c_L \cdot h}} \cdot a = 2.30$  rad, considering the  $\omega$  of the (2,0) mode. We can observe that arching the plate increases the overall stiffness raising the fundamental frequency by a factor 5.23 with respect to the flat case.

### c. Bridge modeling and Comsol SetUp

We now set up the violin model in Comsol and rescale it to obtain a reasonable size of about 35 cm length, 6 cm height and 21 cm width in the larger point. We decided to create a simplified bridge using as main measures the

ones used by most luthiers: 45 mm of height, 38 mm of width and 2.5 mm of thickness. As shown in Figure 1, we started from a scratch rectangular plate and arched both the top and bottom to obtain a bridge that is in contact with the top plate only on the surface of the two feet. Observe that the bridge is positioned in between of the traversal cuts of the f-holes. We then did a form **form assembly** between the violin and the bridge to consider the inefficient boundaries in contact between the two object and used the function **ignore edges** to cancel all useless lines and edges of the model that would ruin the mesh of the violin. The physic chosen for this project is the Solid Mechanics, which permits us to study the mechanical behavior of the violin. For what regards the material, we chose the Sitka Spruce with 12% moisture and set the orthotropic module using the Young's modulus, Poisson's ratio and the shear modulus shown in Table 1.

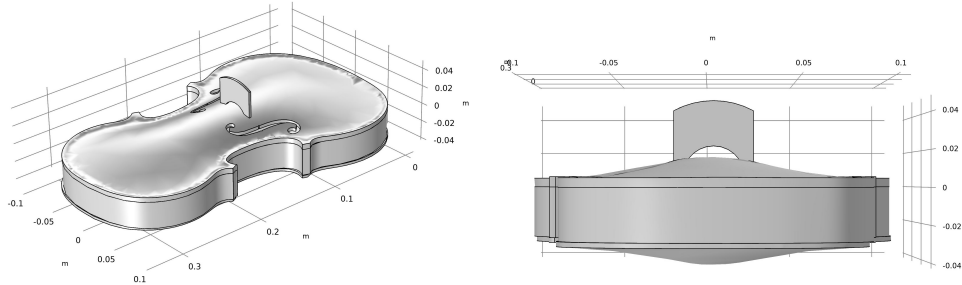


Figure 1: Violin and bridge model

$E_{L(x)}$	12 GPa	$G_{LR}$	0.7 GPa	$\nu_{LR}$	0.37
$E_{R(y)}$	0.9 GPa	$G_{RT}$	0.04 GPa	$\nu_{RT}$	0.43
$E_{T(z)}$	0.5 GPa	$G_{LT}$	0.7 GPa	$\nu_{LT}$	0.47

Table 1: Orthotropic specifics of Young's modulus, shear modulus and Poisson ratio ([1]).

#### d. Eigen-frequency study and plate's mode shapes

Is now time to create a mesh, we decided to apply an user defined mesh with free tetrahedral of size finer, which is surely enough since we will only compute the first five eigen-modes of the back and top plate of the violin. The results are shown in Figures 2 and 3. As several luthiers confirm ([1]), the

main parameter to look at, when the frequency modes of the free plates are calculated, are the frequencies of the X mode (second eigenmode) and ring mode (fifth eigenmode). Furthermore, it is recommendable to have the same frequency one octave higher for the ring mode with respect to the X mode, for both top and back plate. In our case, we obtained a ratio between the fifth and second mode that is in the interval 2.1 – 2.4, which is acceptable.

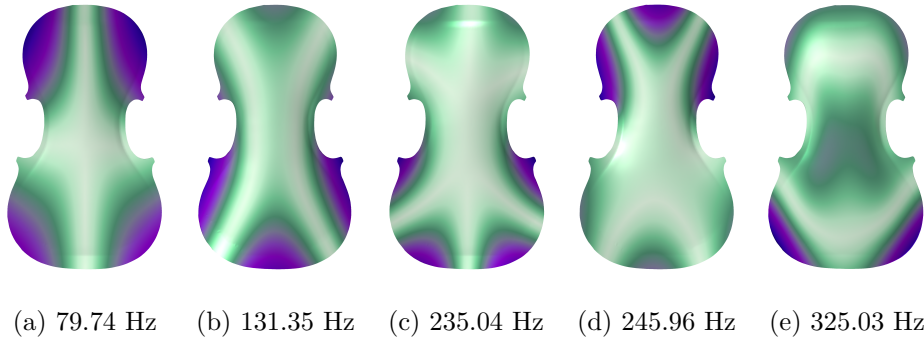


Figure 2: First 5 modes for the backplate

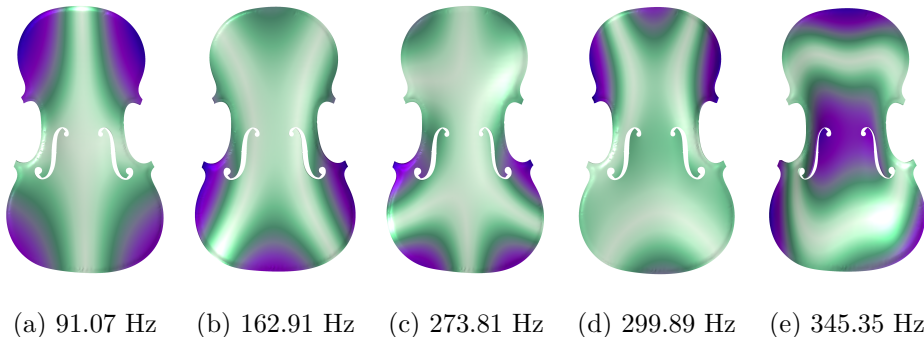


Figure 3: First 5 modes for the backplate

### e. Mobility study

To compute the mobility of the bridge, a point on the top of the bridge was selected and a circular boundary was defined to represent the hammer impact area, as shown in Figure 4. A vertical boundary load of  $f_{tot} = -1$  Newton, applied along the vertical direction of the violin bridge, was then imposed. And a boundary probe was also introduced to measure the average vertical velocity generated by the hammer impact over the boundary.

An extra-fine mesh was used, resulting in a maximum element size of 12.5 mm. Based on this value and assuming a minimum wave speed of 300 m/s., representative of the slowest shear waves in orthotropic spruce, and imposing a minimum of four elements per wavelength leads to a maximum reliable simulation frequency of approximately 6 kHz. However, a wider frequency range from 100 Hz to 10 kHz was analyzed, with a frequency step of 5 Hz. Although the subsequent analysis focuses on a narrower frequency band, this extended range was selected to evaluate the model performance at more critical frequencies.

The resulting mobility, defined as  $Y = \frac{v}{F}$ , is shown in Figure 5. As can be observed, the lower-frequency region presents more distinct mobility peaks, corresponding to frequencies at which the coupled bridge–violin system exhibits a stronger response. Furthermore, the phase response clearly indicates that the system is undamped: at resonance, the phase variations are abrupt. Introducing damping would result in smoother phase transitions and a clearer separation of eigen-frequency modes, especially at higher frequencies.

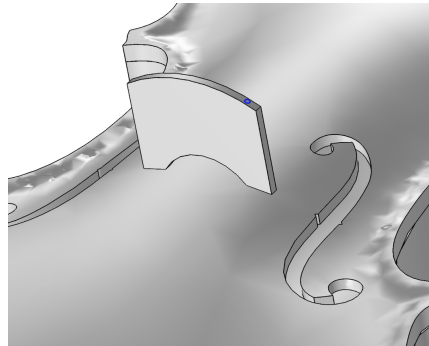


Figure 4: That little blue boundary on the top right of the bridge is the boundary on which the load and probe has been added.

#### f. Frequency Response Function and Coherence

Using the data acquired during the laboratory session, five measurements of the hammer input signals and accelerometer output signals of the violin’s bridge were imported into MATLAB. To all signals an FFT was computed using  $n_{fft} = 8192$  and  $f_s = 96000$  Hz. The power spectral densities of the input  $G_{xx}(f)$ , output  $G_{yy}(f)$  signals and their cross-spectral density  $G_{xy}(f)$  were then computed and averaged across the repeated measurements in order to obtain a more stable estimation of the mobility FRF and reduce the overall

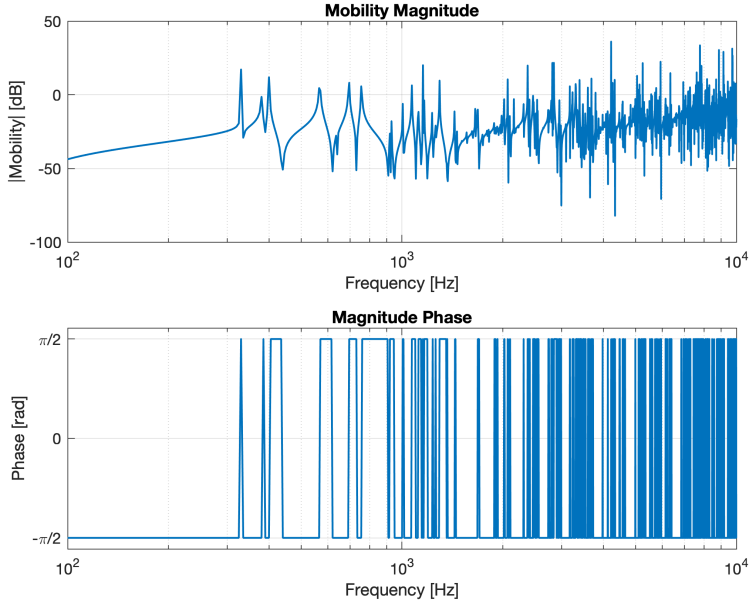


Figure 5: Vertical-Vertical mobility of the bridge obtained through Comsol.

noise. The spectral density have been used to compute the frequency response function and the coherence as shown in equations 1 and 2.

$$\gamma^2(f) = \frac{|G_{xy}(f)|^2}{G_{xx}(f) \cdot G_{yy}(f)} \quad (1)$$

$$Y(f) = \frac{G_{xy}(f)}{G_{xx}(f)} \cdot \frac{1}{j\omega} = \frac{G_{xy}(f)}{G_{xx}(f)} \cdot \frac{1}{j2\pi f} \quad (2)$$

Figure 6 shows the magnitude, phase, and coherence of the averaged laboratory mobility. Based on the coherence values observed in the figure, a frequency range between 200 Hz and 6000 Hz was identified as the interval in which the coherence can be considered acceptable. This frequency range was therefore selected for further analysis and modeling.

As a last observation we can note that at lower frequencies the resonant peaks are much more separated and related with steep negative shifts of the phase.

### g. Filterbank model setup

We now have to design two filterbanks. The first one must have a transfer function that replicates the mobility measured during the lab session. The

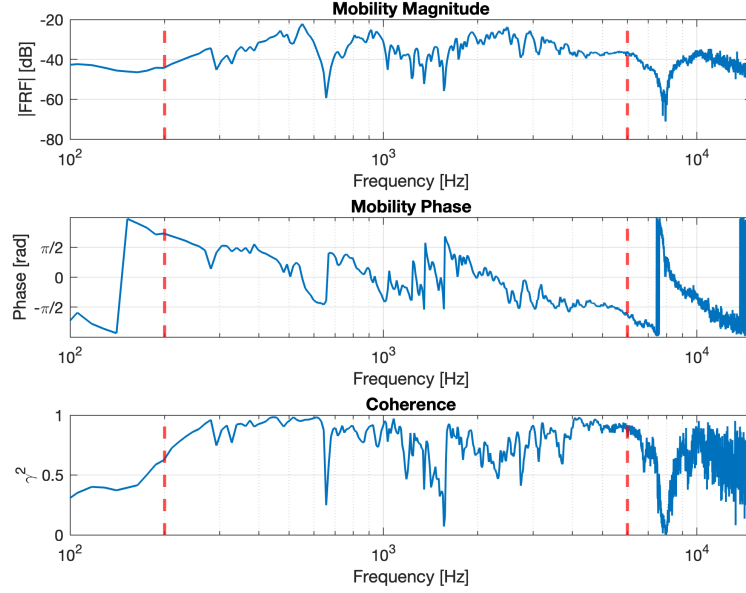


Figure 6: Magnitude, phase and coherence of the mobility average.

second one, instead, must replicate the mobility extracted from the COMSOL simulation.

In order to do so, we have implemented an architecture based on single *RLC* series branches connected in parallel with each other. Each *RLC* series branch acts as a resonator whose center frequency coincides with one of the main peaks in the mobility. The position and shape of each peak is controlled by the values of resistance ( $R$ ), inductance ( $L$ ), and capacitance ( $C$ ). For each resonator, we impose, using the equations in 3, the correct central frequency ( $f_c$ ), half-power bandwidth ( $bw$ ), and the magnitude of the peak maximum ( $H(f_c)$ ).

$$\frac{1}{2\pi\sqrt{LC}} = f_c \quad \frac{R}{2\pi L} = bw \quad \frac{1}{R} = H(f_c) \quad (3)$$

In order to achieve a more accurate identification of the resonance peaks, interpolation was applied to both the experimental and simulated mobility functions.

For the experimental FRF, a total of 17 peaks were taken into consideration. Since the relevance of a peak is not determined only by its global magnitude but also by the behavior around it, we decided to adopt a hybrid methodology. Seven peaks were automatically identified based on a magni-

tude criterion. However, because the peaks with the highest magnitude were concentrated in the upper part of the spectrum, this approach did not adequately represent the lower-frequency region of the mobility. For this reason, an additional 10 peaks were manually selected in order to better describe the response in frequency ranges where a purely magnitude-based selection would fail. The same approach was applied on the COMSOL mobility, for a total of 21 peaks. Once the filterbanks have been created we fed them with an impulse signal to obtain as a result the impulse response functions of the circuits. The simulated FRF are finally shown in Figures 7 and 8. In the COMSOL plot it's clearly visible a decaying trend of the phase: this is a cumulative effect of having many resonators close to each others, which happens mainly at higher frequencies.

It is noticeable that the selection of the peaks is a delicate part, because it dictates the parts in which the violin mobility is better simulated.

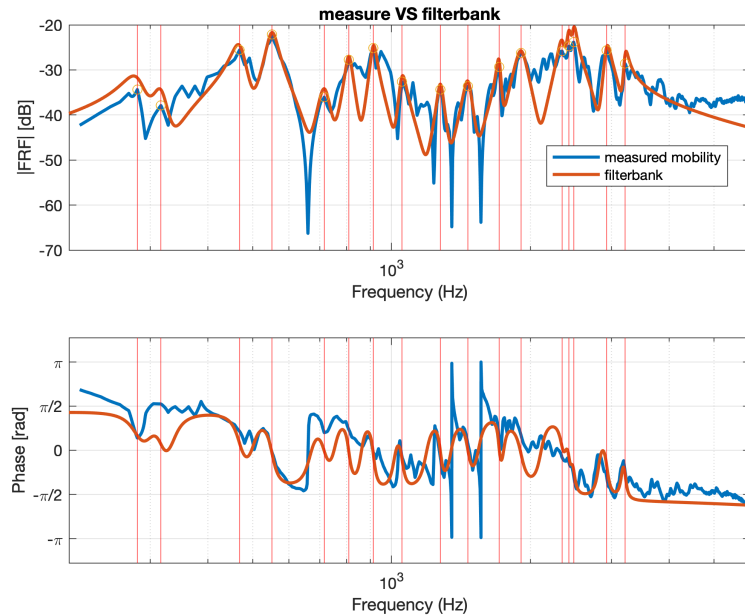


Figure 7: RLC simulation of Lab Mobility.

For the sake of brevity, the RLC systems implemented in Simulink are not reported here and are available on [GitHub](#).

#### h. Karplus-Strong's excitation signal study

The Karplus-Strong algorithm was adopted to simulate the excitation of a plucked string at the bridge. Using the diagram in Figure 9 we replicated

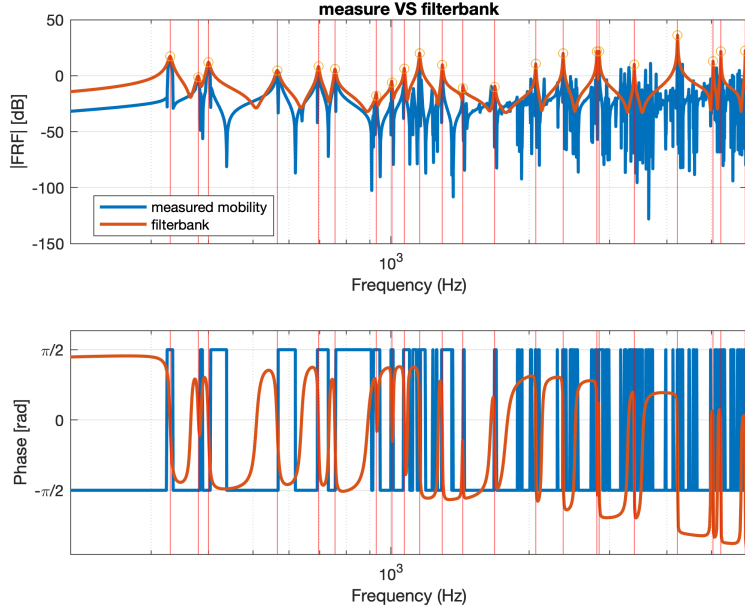


Figure 8: RLC simulation of Comsol Mobility.

such algorithm in MATLAB choosing the following parameters:

- Fundamental frequency  $f_0 = \frac{F_s}{m} = 440$  Hz.
- Gain value  $g = 0.99$ , in order to obtain a strong presence of the delayed signal with respect to the input signal and to ensure a sufficient stability of the overall filter.

A low-pass filter was included inside the feedback path in order to introduce frequency-dependent losses, resulting in faster decay of higher harmonics and an overall smoother response.

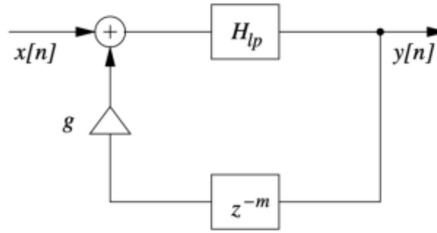


Figure 9: Block scheme of the Karplus-Strong system.

The input signal used to excite the system consists of a 1-second long white noise segment, followed by zero padding. The noise provides the initial

excitation of the system, while the zero-padding allows the feedback loop to decay without input, reproducing the damped oscillations of a plucked string.

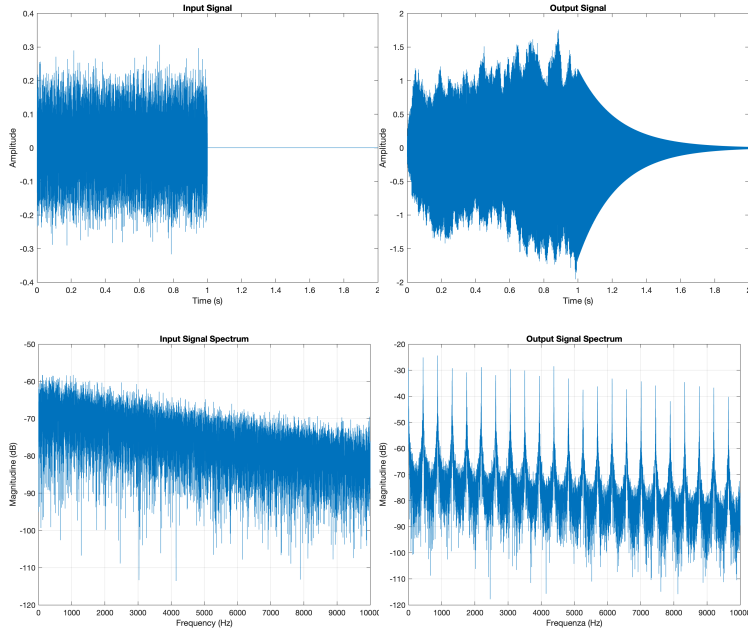


Figure 10: Input and output in time and frequency of the Karplus–Strong filter with  $f_0 = 440$  Hz and sampling frequency  $F_s = 96000$  Hz.

Figure 10 shows the time-domain signals and magnitude spectra of the input and output. The output signal exhibits evident harmonics and a frequency-dependent decay caused by the feedback loop.

Using the Karplus–Strong algorithm described above, a string-like excitation was applied to the filterbanks. The resulting outputs are shown in Figure 11, while the audio files obtained are available on [GitHub](#). As expected the electric circuit acts as a filter on the input signal, boosting its natural frequencies.

The two solutions clearly differ when comparing both the graphs and associated audio files. In the COMSOL case, the peaks identified along the filterbank response are more sharply defined, corresponding to a much higher quality factor  $Q$ , while the peaks observed in the laboratory case appear significantly smoother, as expected in a real scenario where multiple energy dissipation mechanisms are present. This difference can be attributed to the fact that, in the numerical model, effects such as sound absorption due to wood and varnish, non-ideal boundary conditions, and experimental measurement limitations are simplified or not fully accounted for. Referring to the audio

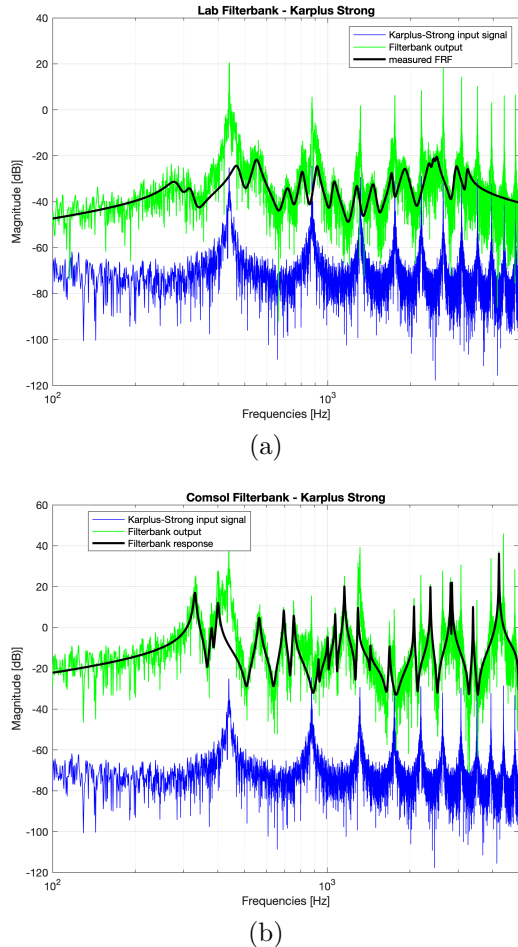


Figure 11: (a) K-S through model-like filterbank; (b) K-S through measure-like filterbank.

files, the one referred to the lab measurements is more similar to the sound of an actual wooden violin. The discriminant factor between the two is the filterbank approximation of the FRF to a measured mobility, which was not very reliable in the first place. Another key aspect is the fact that the resulting sound is one we could obtain if we "listen" with the ear placed on the bridge of the violin: this audio file lacks many aspects of the complete radiation of the instrument, thus resulting in an incomplete vision of the violin's characteristic tone.

## References

- [1] Neville H. Fletcher and Thomas D. Rossing. *The Physics of Musical Instruments*. Springer-Verlag, 1991.